Simultaneous bond-selective deuterium-based isotopic labeling sensing with disposable ultra-miniature CARS fiber probe

TONG WANG,[1,2,3] JUNFENG JIANG,[1,2,3,*] KUN LIU,[1,2,3]
SHUANG WANG,[1,2,3] TIANHUA XU,[1,2,3,4] PANPAN NIU,[1,2,3]
JINYING MA,[5] JINDE YIN,[6] AND TIEGEN LIU[1,2,3]

[1]*School of Precision Instrument and Opto-Electronics Engineering, Tianjin University, Tianjin 300072, China*

[2]*Key Laboratory of Opto-Electronics Information Technology (Tianjin University), Ministry of Education, Tianjin 300072, China*

[3]*Tianjin Optical Fiber Sensing Engineering Center, Institute of Optical Fiber Sensing of Tianjin University, Tianjin 300072, China*

[4]*School of Engineering, University of Warwick, Coventry CV4 7AL, United Kingdom*

[5]*School of Electronic Engineering, Tianjin University of Technology and Education, Tianjin 300222, China*

[6]*Shenzhen Nuoan Technology Co. Ltd., Shenzhen 518107, China*

[*]jiangjfjxu@tju.edu.cn

Abstract: Deuterium-based isotopic labeling is an important technique for tracking cellular metabolism with the Raman signals analysis of low-wavenumber (LW) C–D bonds and high-wavenumber (HW) C–H bonds. We propose and demonstrate a disposable ultra-miniature fiber probe to detect LW and HW coherent anti-Stokes Raman scattering (CARS) spectra for deuterated compounds simultaneously and bond-selectively sensing. The 10.78 µm diameter disposable fiber probe, comprised of focusing taper as fiber probe head and time-domain walk-off eliminating fiber section with designed length, realizes wide-frequency-interval dual Stokes pulse delivering and focusing. The fiber probe enables quantitative concentration determination with resolution down to 11 mM. The chemical vibration modes of LW region C–D bonds and HW region C–H bonds of the mixture samples of organic compounds and their deuterated counterparts in a simulated cell are simultaneously excited and characterized. The CARS disposable fiber probe introduces a promising handle for in vivo biochemical detection based on isotopic labeling sensing.

1. Introduction

Stable isotope labeling is widely used as a tracer in biological, medical, pharmaceutical, and environmental fields through the study of metabolic fluxes [1–3]. The stable isotope, specifically [2]D, substantially participates in cellular metabolic activities by replacing their primordial isotopes, and thus cellular metabolic activity can be revealed by monitoring the intracellular conversion of element ^{1}H to its isotope [2]D. For example, tracking the glucose uptake in the metabolic pathways and the diverging allocation of glucose towards the synthesis of various macromolecules (such as nucleic acids, glycogen, protein, and lipids) can distinguish foam cells from activated macrophages and vascular smooth muscle cells and have potential significance for unraveling the pathogenesis of atherosclerosis plaques [4–7]. Stable isotope tracer methods combined with conventional mass spectrometry (MS) and nanoscale secondary ion mass spectrometry (nano-SIMS) allow quantification of stable isotope tracers at sub-organelle resolution and show significant heterogeneity of glucose metabolism in foam cells, macrophages, and VSMCs in atherosclerosis [8–10]. However, the limitations of atomic weight- and nuclear spin-based detection mechanisms prevent them from fully and accurately obtaining precise molecular

structure information and restrict them to only probing the early processes of glucose metabolism, including fluxes that are taken up or converted to small-molecule metabolites [11,12]. Besides that, MS and nano-SIMS require special preparation of the sample, such as extraction, enrichment, or derivatization, which can be time-consuming and introduce potential errors [13]. Nano-SIMS requires the sample to be placed in a vacuum environment, which may affect the biomorphology and the activity of the sample [14,15]. The later processes of glucose anabolic products towards macromolecule synthesis remain a gap to these techniques.

Raman spectroscopy can detect the stable labeled compounds within cells by characterizing the vibrational modes of the chemical bonds. Benefiting from the label-free and non-destructive nature of Raman spectroscopy, detection can be performed inside living cells without pre-processing [16]. The strategy to identify isotopically substituted molecular species is to detect the frequency downshift of the chemical bonds in the Raman spectra. For the deuterium-based isotope, the Raman peak downshift from high-wavenumber (HW, 2800–3100 cm^{-1}) region to low-wavenumber (LW, 1800–2300 cm^{-1}) region as the C–H bonds are converted to C–D bonds. The downshift values depend on the specific C–H or C–D vibrational modes that are being explored, as well as on the nature of the surrounding chemical environment [17]. The downshift values are typically ∼800 cm^{-1}. Consequently, the capability to detect a broad Raman band or wide interval Raman band is crucial. The Raman spectroscopy combined with isotope labeling can reveal the cellular metabolism by monitoring the changes of the C–H bonds and C–D bonds and is applied for antibiotic susceptibility testing of infecting bacteria cells [18], detection of viable but nonculturable bacteria cells [19], tracing the metabolism of lipids and their storage patterns in eukaryotic cells [20–22]. However, the tiny scattering cross-section of Raman scattering requires long spectra acquiring time to enhance the signal level, which limits its real-time monitoring potential.

The inherently weak spontaneous Raman signal can be increased by many orders of magnitude through surface-enhanced Raman scattering (SERS) and coherent Raman scattering (CRS). In SERS, target stable isotopes are attached to silver or gold surfaces for the enhancement of the Raman signal, which introduces an external interference in the spectra reproducibility challenge [23]. CRS, including stimulated Raman scattering (SRS) and coherent anti-Stokes Raman scattering (CARS), directly enhances the weak Raman signals and offers a nature high specificity by exploiting the non-linear effect that happens when the frequencies of the two excitation pulses match with the target chemical bonds. SRS detection mechanism cannot achieve backward detection while CARS generates both forward and backward signals, making CARS preferred in endoscopy-like scenarios. The drug response of live cells to deuterated docosanol was investigated with the multiplex CARS [24]. Nevertheless, the supercontinuum-spectra-based multiplex CARS has a low energy density in each wavenumber and needs a large total optical power for covering a broad Raman range, resulting in a limited signal level improvement potential. Switching-CARS or fast-tunable-frequency-CARS detect Raman signals of two or multiple vibration modes with higher optical efficiency. LW and HW Raman spectra are detected by switching between two wavelengths of Stokes pulses at high speed, so the detection is quasi-simultaneity [25,26]. Dual-frequency Stokes pulses are promising to realize true simultaneity. Dual-frequency Stokes pulses can be generated with the birefringent effect of polarization-maintaining photonic crystal fiber (PM-PCF) [27–29]. However, the anomalous dispersion and birefringence of the PM-PCF inevitably introduce a time-domain walk-off for Stokes pulses with large optical frequency intervals, which require pump pulse to switch between two-time delay line positions or to split spatially into two-time delay paths. Furthermore, the microscope objective lens is used as a probe head, making the system bulky, complex, and unsuitable for *in vivo* detection. Compared to traditional bulky optic probes, miniature fiber optic probes are smaller, less expensive, and more suitable for fabricating disposable fiber probes and biomolecule detection [30,31].

In this paper, we propose and demonstrate an ultra-miniature disposable fiber probe that simultaneously and bond selectively detects the deuterated compounds' LW and HW region CARS spectra. The disposable fiber probe, comprised of focusing taper as fiber probe head and time-domain walk-off eliminating fiber section, realizes wide-frequency-interval dual Stokes pulse delivering and focusing, as shown in Fig. 1(b). For selected chemical bonds, the disposable fiber probe is customized to a suitable length to eliminate the time-domain walk-off of the wide-frequency-interval dual-pulse. The capability of fiber probes to simultaneously detect LW and HW region CARS spectra is demonstrated by the characterization of ethanol/benzonitrile mixture in a simulated cell. The potential of the disposable probe for isotope labeling applications is then verified by probing compounds and their deuterated counterparts. The all-fiber format probe compensates the time-domain walk-off of the Stokes wide-frequency-interval dual-pulse without bulky optics, making the LW and HW region CARS signal detection flexible and cost-effective. The proposed CARS disposable fiber probe brings one step closer to the practicality of *in vivo* biochemical detection combined with stable isotope probing.
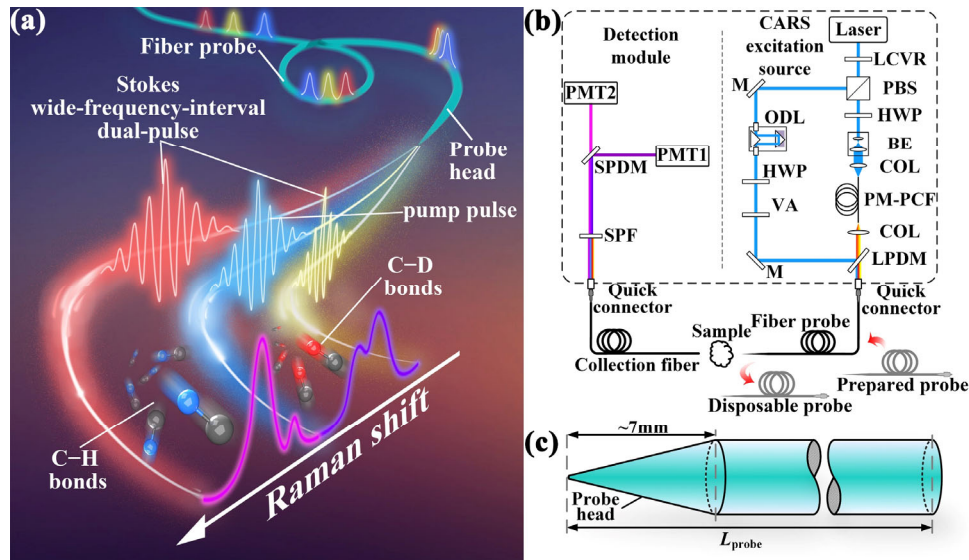

Fig. 1. Schematic diagram of simultaneous bond-selective deuterium-based isotopic labeling sensing. (b) Schematic diagram of the experimental setup, including CARS excitation source and detection module. LCVR: liquid crystal variable retarder, PBS: polarization beam splitter, HWP: half-wave plate, BE: beam expander, FP: fiber-port, PM-PCF: polarization-maintaining photonic crystal fiber, COL: collimator, M: mirror, ODL: optical delay line, VA: variable optical attenuator, LPDM: long-pass dichroic mirror, SPDM: short-pass dichroic mirror, PMT: photomultiplier tube, SPF: short pass filter. (c) The structure of CARS fiber probe. The fiber probe is made of few-mode fiber and the L_{probe} is 51.64 cm.

2. Materials and methods

2.1. *Stokes wide-frequency-interval dual-pulse generation*

The wide-frequency-interval dual-pulse is necessary to detect LW and HW region CARS signals simultaneously. Dual-soliton pulses generated by the PM-PCF (NL-PM-750, NKT Photonics) can serve as Stokes wide-frequency-interval dual-pulse. The dual-soliton pulses are generated by injecting linear polarization femtosecond pulses into the PM-PCF. The wavelengths of the dual-soliton pulses can be tuned by adjusting the optical power and the linear polarization

orientation of the incident pulses. The details of the Stokes wide-frequency-interval dual-pulse generation can be found in the Supplement 1 and Ref. [32].

The homemade Stokes wide-frequency-interval dual-pulse CARS excitation setup is shown in Fig. 1(b). A fiber-based laser source (C-fiber 780, MenloSystems) with a 70 mW average power output at 100 MHz repetition rate is used. The pulse duration, central wavelength, and spectral bandwidth are 80.49 fs, 780 nm, and 12.82 nm, respectively. The output laser pulse is split into pump and Stokes paths using a liquid crystal variable retarder (LCC1113-B, Thorlabs) and a polarization beam splitter (PBS, PBS052, Thorlabs). A motorized optical delay line (ODL100/M, Thorlabs) is inserted into the pump path. It is worth noting that the optical delay line needs no movement during the simultaneous detection of LW and HW region when the disposed fiber probe length is customized according to selected bonds. The pump and Stokes pulses are combined by a long-pass dichroic mirror (cutoff wavelength: 900 nm, LPDM900, Thorlabs). In this manuscript, the center wavelength of the Stokes wide-frequency-interval dual-pulse is tuned to 948 nm and 1031 nm, respectively, and the spectrum is shown in Fig. 2(a).
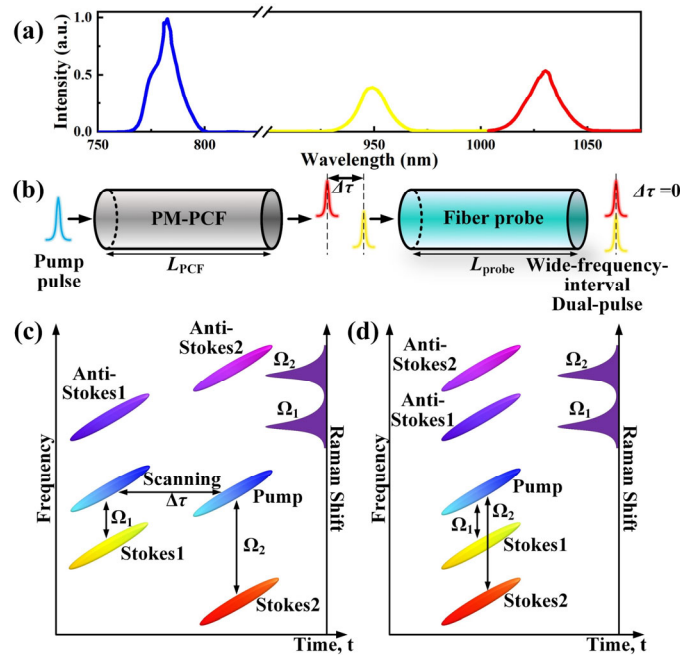

Fig. 2. (a) The wavelength of the Stokes wide-frequency-interval dual-pulse is tuned to 948 nm and 1031 nm, and the wavelength of the pump pulse is 780 nm. (b) An optical time delay $\Delta\tau$ exists between dual-Stokes pulses generated by the PM-PCF, and can be eliminated by the fiber probe. (c) The schematic diagram of the method for measuring $\Delta\tau$. (d) LW and HW region CARS signals can be simultaneously excited after pulse-to-pulse alignment.

2.2. *Stokes wide-frequency-interval dual-pulse time-domain alignment*

The dual-soliton pulses serving as Stokes wide-frequency-interval dual-pulse are temporally non-overlapping due to the anomalous dispersion and the birefringence effect of the PM-PCF. Pulse-to-pulse alignment is required to achieve simultaneous LW and HW region CARS signals detection.

A time-domain walk-off $\Delta\tau$ exits between dual-soliton pulses with different wavelengths, as shown in Fig. 2(b) and (c), resulting in the pump pulse necessitating being split into two parts

that temporally overlap with the dual soliton pulse, respectively. The time-domain walk-off $\Delta\tau$ consists of two parts, τ_1 and τ_2. The time-domain walk-off τ_1, caused by the anomalous dispersion of the PM-PCF, is wavelength-dependent. The birefringence effect of the PM-PCF causes the time-domain walk-off τ_2, which can be regarded as wavelength-independent. When the soliton pulse with a larger wavelength corresponds to the fast-axis of the PM-PCF and the soliton pulse with a smaller wavelength corresponds to the slow-axis, the relative time-domain walk-off between dual-soliton pulses is $\Delta\tau_a = \tau_1 - \tau_2$. Otherwise, the relative time-domain walk-off is $\Delta\tau_b = \tau_1 + \tau_2$.

The wavelength-dependent time-domain walk-off τ_1 caused by the anomalous dispersion of the PM-PCF can be calculated by the general non-linear Schrödinger equation (GNLSE) [33]. The optical time time-domain walk off τ_2 caused by birefringence is [34]:

$$\tau_2 = \frac{B \times L}{c} = \frac{\Delta\tau_b - \Delta\tau_a}{2} \tag{1}$$

B and L_{PCF} are the birefringence coefficient and the length of the PM-PCF, and c is the speed of light. Adding a suitable length L_{probe} of fiber probe with normal dispersion can generate $-\Delta\tau$ for time-domain alignment, as shown in Fig. 2(b) and (d).

2.3. Reagents and materials

The samples used in the experiments, benzonitrile (Catalog No. B803712), ethanol (Catalog No. E809061), cyclohexane (Catalog No. C804200), acetone-d6 (Catalog No. A800097), methanol (Catalog No. M813907), and methanol-d4 (Catalog No. M812878), were purchased from Macklin Biochemical Co., Ltd. (Shanghai, China). Cyclohexane-d12 (Catalog No. C-70391 G) was purchased from Heowns Biochemical Technology Co., Ltd. (Tianjin, China). Acetone (Catalog No. 0000184) was purchased from Rionlon Chemical Co., Ltd. (Tianjin, China).

For quantitative key-selective identification, samples were prepared by mixing benzonitrile and ethanol in different proportions. Because benzonitrile possesses two independent Raman resonances in LW and HW Raman spectra, while ethanol possesses Raman resonances only in HW Raman spectra. For stable isotope labeling application, the samples used in the experiments included three organic compounds, cyclohexane, acetone, and methanol, and their deuterated counterparts, cyclohexane-d12, acetone-d6, and methanol-d4. The cyclohexene/cyclohexene-d12 mixture, acetone/acetone-d6 mixture, and methanol/methanol-d4 mixture are prepared by directly incorporating organic compounds into the corresponding deuterated counterparts.

2.4. Fiber probe design and fabrication process

The disposable fiber probe used in the experiments is made of graded-index few-mode fiber (FMF, FM GI-4, YOFC). The core and cladding diameters of the FMF are 23 μm and 125 μm, respectively. Compared to other solid core fibers, the four-wave mixing signal of the FMF signal does not interfere with the measurement of the C-H bonds CARS signals [35].

The disposable fiber probe is fabricated into an adiabatic taper by the hydrogen/oxygen flame brushing technique. The adiabatic taper possesses a smooth taper-transition region, allowing the excitation pulses to remain in fundamental mode. The process steps are: (1) removing the coating layer of the FMF and fixing it to the fixture; (2) Continuous heating and stretching of the FMF to the proper length using a flame; (3) finding and measuring the diameter of the thinnest position of the FMF, and slicing it into two parts by using the fiber splicing system (LDS 2.5, 3SAE). The structure of the disposable fiber probe is shown in Fig. 1(c). The 7 mm long, 10.78 μm diameter fiber probe head is fabricated by the hydrogen/oxygen flame brushing technique, and the L_{probe} is 51.64 cm.

3. Experimental results

3.1. *Time-domain walk-off measurement*

The schematic diagram of the method for measuring $\Delta\tau$ is shown in Fig. 2(d). For the measurement of $\Delta\tau$, the benzonitrile with two independent Raman resonant peaks at 2230 cm^{-1} and 3073 cm^{-1} is used as the standard sample. For the 2.81 m PM-PCF used in our experiments, the wavelength-dependent coefficient of time-domain walk-off is 0.137 ps/nm [36]. The time-domain walk-off τ_1 of the Stokes wide-frequency-interval dual-pulse with wavelengths of 948 nm and 1031 nm, respectively, is 11.371 ps.

The CARS signals collection system is shown in Fig. 3(a). The pump pulses and Stokes wide-frequency-interval dual-pulse are focused on the samples by the 20× objective lens (N20X-PF, Nikon). The forward CARS (F-CARS) signals are collected by another objective lens, filtered out from the excitation pulses by a short-pass filter (cutoff wavelength 750 nm, FESH0750, Thorlabs), and detected by a photomultiplier tube (PMT, PMM02, Thorlabs). The measured CARS signals of benzonitrile without a normal dispersion medium are shown in Fig. 3(b). The relative optical delay is calculated to be $\Delta\tau_a = 3.15$ ps, and $\Delta\tau_b = 19.6$ ps. Thus, the optical time delay τ_2 is 8.225 ps, and the birefringence coefficient of PM-PCF is 8.78×10^{-4}.
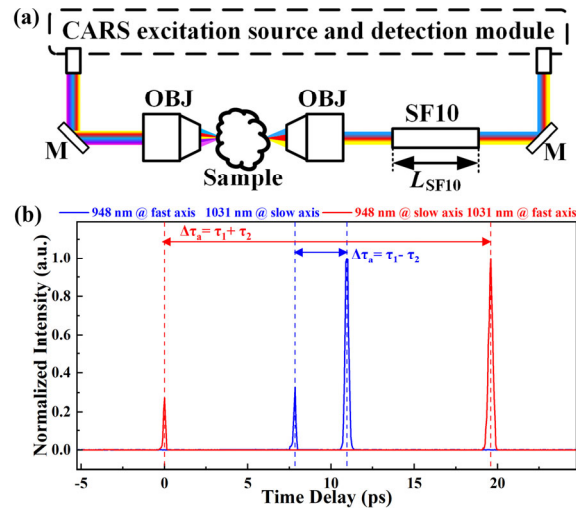

Fig. 3. (a) The experimental setup for measuring optical time delay $\Delta\tau$. SF10: SF10 dispersion glass rod, OBJ: objective lens. (b) The measured optical time delay $\Delta\tau$ without normal dispersion medium.

The normal dispersion medium SF10 glass rod is then added to the Stokes path to verify if the time-domain walk-off could be reduced or even eliminated. For Stokes wide-frequency-interval dual-pulse with wavelengths of 948 nm and 1031 nm, the time-domain shift introduced by the SF10 glass rod is –0.08225 ps/cm. SF10 glass rods with lengths L_{SF10} being 5 cm, 10 cm, 15 cm, and 20 cm are inserted in sequence, and the measured time-domain walk-off $\Delta\tau_a$ is 2.75 ps, 2.35 ps, 1.92 ps, and 1.50 ps under corresponding glass rod lengths, while $\Delta\tau_b$ is 19.18 ps, 18.77 ps, 18.42 ps, and 18.00 ps, as shown in Fig. 4. The measured results demonstrate that the time-domain offsets $\Delta\tau_a$ and $\Delta\tau_b$ decrease as the L_{SF10} increases.

3.2. *Disposable fiber probe simultaneously detects LW and HW region CARS spectra*

The experimental system is established according to Fig. 1(b) and the photograph of the disposable fiber probe is shown in Fig. 5(a). The spectral focusing method is applied in CARS signals
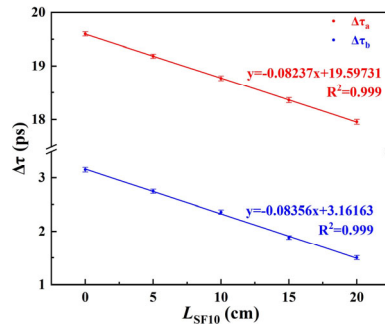
Fig. 4. The measured CARS signals of benzonitrile when adding 0 cm, 5 cm, 10 cm, 15 cm, and 20 cm SF10 glass rods into the system.

measurement to improve the spectral resolution. The chirped pump pulses and Stokes wide-frequency-interval dual-pulse generated by the CARS excitation source are injected into the disposable fiber probe through a collimator (PAF-X-7-B, Thorlabs). Different Raman vibration spectra can be measured when the different frequency components of the pump and Stokes wide-frequency-interval dual-pulse overlap. LW and HW region CARS spectrum can be obtained by shifting the optical delay line to shift the pump pulse in time. The disposable fiber probe outputs the tightly focused pulses to irradiate the sample and excite the F-CARS signal. The generated F-CARS signals of samples are collected by an FMF and filtered out from the excitation pulses by a short-pass filter (cutoff wavelength 750 nm, FESH0750, Thorlabs). A short-pass dichroic mirror (SPDM, cutoff wavelength: 650 nm, SPDM650, Thorlabs) is added to the signal collection side to separate the simultaneously generated LW and HW region CARS signals system. The reflectance of SPDM for anti-Stokes light with wavelengths less than 646 nm and the transmittance of anti-Stokes light with wavelengths greater than 660 nm are both greater than 90%. The LW region CARS signal ($<2400 \, \text{cm}^{-1}$) is reflected by the SPDM and detected by PMT1, while the HW region CARS signal ($>2700 \, \text{cm}^{-1}$) is transmitted by the SPDM and detected by PMT2. The signal from the PMT is sent to a data acquisition card (NI 6356, National Instruments). The input range is ±2 V and the ADC resolution is 16 bits.

The disposable fiber probe is fabricated with normal dispersion fiber, which is comprised of focusing taper as fiber probe head and time-domain walk-off eliminating fiber section for precise alignment of the Stokes wide-frequency-interval dual-pulse. The length of the optical fiber is customized according to the specified Stokes wide-frequency-interval dual-pulse based on the selected chemical bonds. The disposable fiber probe delivers the CARS excitation pulses into the sample directly and closely, making it particularly suitable for *in vivo* testing. The time-domain shift coefficient caused by FMF (FM GI-4, YOFC) is –0.735 fs/(nm·cm). When the 1031 nm Stokes pulse corresponds to the fast-axis of the PM-PCF and the 948 nm Stokes pulse corresponds to the slow-axis, 51.64 cm FMF can align the Stokes wide-frequency-interval dual-pulse generated by the 2.81 m PM-PCF, and realize simultaneous LW and HW region CARS detection. The end of the FMF is fabricated into an adiabatic taper as a disposable fiber probe head using the hydrogen/oxygen flame brush technique. The length of the fiber probe head is 7 mm, and the end diameter is 10.78 µm, as shown in Fig. 5(b).

To demonstrate the ability of the disposable probe to measure down to a single cell, an 80 µm outer diameter hollow glass microbubble fixed on a hold fiber served as the simulated cell to be detected. A 10 µm diameter injector injects different liquids simulating cytoplasm into the simulated cell. The disposable probe is mounted on a three-dimensional manipulator to point at the simulated cell, and delivers the CARS excitation lights to the simulated cell. The micrograph of the fiber probe probing a simulated cell is shown in Fig. 5(c) and (d). We
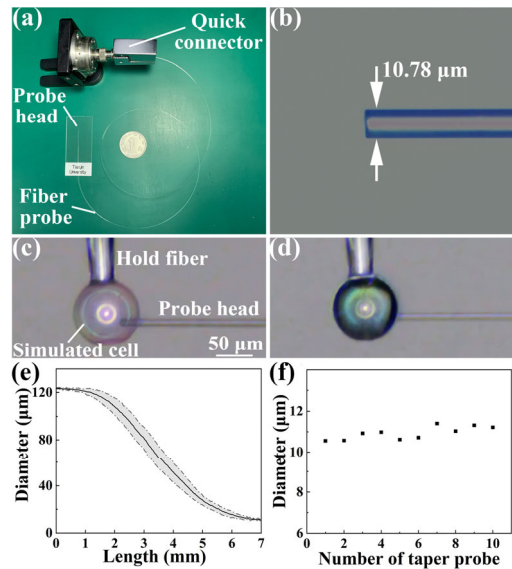
Fig. 5. (a) Photograph of the disposable fiber probe setup, including a quick connector and the fiber probe. The excitation pulses are coupled into the end of the fiber probe via the quick connector. (b) Micrograph of the fabricated fiber probe head. The excitation pulses transmit in the fiber probe and finally focus by the 10.78 μm diameter probe head. The disposable probe probing a (c) empty and (d) filled simulated cell. The simulated cell is fixed on a hold fiber, and the filled contents in the simulated cell are injected by a micropipette (not shown in the diagram). (e) The outer diameters of the fiber probes at different positions. (f) The diameters of tapered optical fiber probes.

fabricated ten tapered optical fiber probes with 7 mm length. The outer diameters of the fiber probes at different positions are shown in Fig. 5(e), and the fabricated fiber probes are relatively uniform. The infrared camera of the fiber splicing system has a measurement accuracy of 1 μm, and thus the measured diameters of fiber probes at the 7 mm position are all about 11 μm. The actual diameters of tapered optical fiber probes are measured by the microscope, as shown in Fig. 5(f). The fabricating accuracy is ±0.5 μm. The reproducibility of the fiber probes indicates the feasibility of mass production. We placed the fiber optic probe in the air medium and captured the cross-sectional imaging of 780 nm, 948 nm, and 1031 nm laser spot output from the disposable fiber probe. The cross-sectional imaging and the intensity profiles are shown in Fig. 6. The spot size of the 780 nm, 948 nm, and 1031 nm laser spot is 9.93 μm, 10.32 μm, and 10.41 μm. The size of the focused spot using fiber probe is relatively large compared to the traditional objective-based probes, making the sensitivity relatively low. Future work will reduce the fiber probe end size and spot size to improve the excitation pulse intensity and the CARS signal intensity.

We first demonstrate the capability of the disposable probe to simultaneously detect LW and HW region CARS signals by injecting an ethanol, a benzonitrile, and a 1:1 ethanol/benzonitrile mixture into the simulated cell. The measured LW and HW region CARS spectra of the samples are shown in Fig. 7(a). When the ratio of ethanol and benzonitrile is 1:0, the measured CARS spectrum is shown as the solid red line in Fig. 7(a). In the HW region, the Raman resonance peak of ethanol at 2876 cm^{-1} is visible, while the Raman resonance peaks at 2927 cm^{-1} and 2973 cm^{-1} of ethanol are displayed in one peak due to the limited resonance spectral resolution of our present CARS system and the weak energy of the Raman resonance peak at 2973cm^{-1}. The disposable probe measure Raman resonance spectra with a resolution of ~50 cm^{-1}. The
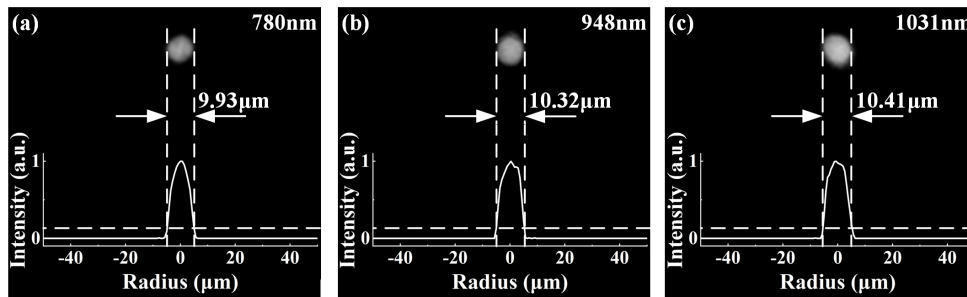
Fig. 6. The cross-sectional imaging and the intensity profile of (a) 780 nm, (b) 948 nm, and (c) 1031 nm laser spot output from disposable fiber probe. The background medium is air.

absence of Raman resonance peaks in the LW region is consistent with the spontaneous Raman scattering spectrum of ethanol. When the ratio of ethanol and benzonitrile is 0:1, the measured CARS spectrum is shown as the solid blue line in Fig. 7(a). The Raman resonance peak of benzonitrile can be seen at $3073\,cm^{-1}$ in the HW region and $2230\,cm^{-1}$ in the LW region, which is consistent with the spontaneous Raman scattering spectrum of benzonitrile. When the ratio of ethanol to benzonitrile is 1:1, the Raman resonance peaks of benzonitrile and ethanol in the LW and HW regions are detected simultaneously, as shown by the solid green line in Fig. 7(a). The intensity of Raman resonance peaks at $2230\,cm^{-1}$ in the LW spectra I_{2230} and $3073\,cm^{-1}$ in the HW spectra I_{3073} increased as the ratio of benzonitrile in the mixture increased, As shown by the solid blue line in Fig. 7 (b) and (c). The intensity of Raman resonance peaks at $2876\,cm^{-1}$ in the HW spectra I_{2876} decreased as the ratio of ethanol in the mixture decreased, as shown by the solid red line in Fig. 7(c). The peak intensities at $2230\,cm^{-1}$, $2876\,cm^{-1}$, and $3073\,cm^{-1}$ varied by 16.4 mV, 18.5 mV, and 26 mV, respectively, over the 50%~100% concentration range. A linear fitting is executed in the concentration range of 50~100%, and the calculated measurement resolution of the peaks at $2230\,cm^{-1}$, $2876\,cm^{-1}$, and $3073\,cm^{-1}$ is 0.186% (18 mM), 0.165% (28 mM) and 0.117% (11 mM), as shown in Fig. 7(b) and (c). Our probe is simple to fabricate, cost-effective, and has a wide detection range.

Then, we move to organic compounds and their deuterated counterparts to demonstrate the capability of the disposable probe for stable isotope labeling applications. The number in the name of the deuterated counterparts represents the number of ^{1}H replaced by ^{2}D in a single molecule. For example, in a single cyclohexane-d12 molecule, twelve ^{1}H are substituted by ^{2}D, and twelve C–H bonds in cyclohexane are substituted by C–D bonds. Three organic compounds and their deuterated counterparts are utilized as samples and injected into the simulation cell. Figure 8(a) shows the measured CARS spectra of the cyclohexane/cyclohexane-d12 mixture injected into the simulated cell. Two Raman resonance peaks exist in the HW spectra, the Raman resonance peak at $2853\,cm^{-1}$ represents symmetric CH_2 stretching vibration, and the other Raman resonance peak contains $2923\,cm^{-1}$ and $2938\,cm^{-1}$ represents asymmetric CH_2 stretching vibration in the cyclohexane. The replacement of ^{1}H by ^{2}D in cyclohexane-d12 results in a decrease in the molecular vibrational frequency. Three Raman resonance peaks exist in the LW region CARS spectra, two Raman resonance peaks at $2155\,cm^{-1}$ and $2200\,cm^{-1}$ represent asymmetric CD_2 stretching vibration, and the other peak contains the Raman resonance at $2083\,cm^{-1}$ and $2106\,cm^{-1}$ represents symmetric CD_2 stretching vibration. Figure 8(b) shows the measured CARS spectra of the acetone/acetone-d6 mixture injected into the simulated cell. In HW spectra, the Raman resonance peak at $2921\,cm^{-1}$ represents symmetric CH_3 stretching vibration in the acetone. In the LW spectrum, two Raman resonance peaks representing symmetric CD_3 vibration in acetone-d6 are at $2111\,cm^{-1}$ and $2184\,cm^{-1}$. Figure 8(c) shows the measured CARS spectra of the methanol/ methanol-d4 mixture injected into the simulated cell. Two
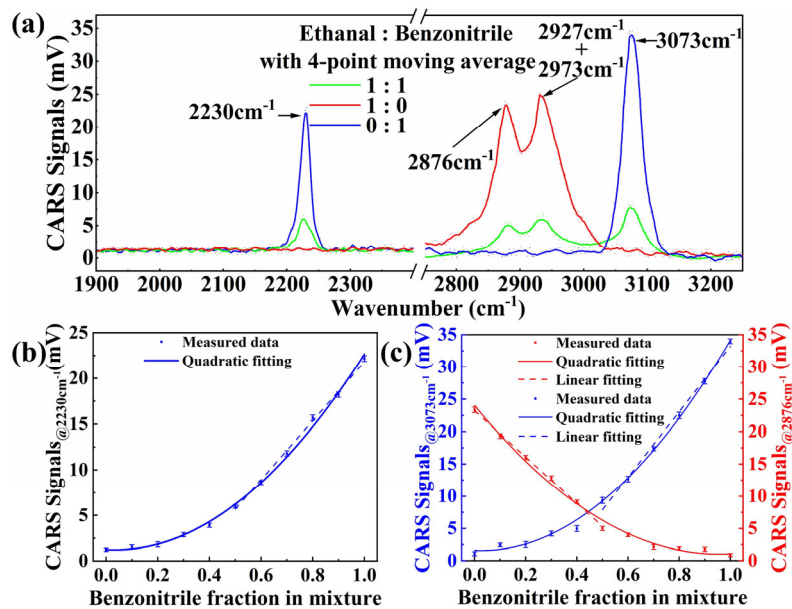
Fig. 7. a) The measured LW and HW region CARS spectra of the ethanol (red trace), benzonitrile (blue trace), and 1:1 ethanol/benzonitrile mixture (green trace). (b) CARS signal intensity of I_{2230} in the mixture and theoretical fitting curve as a function of benzonitrile fraction in benzonitrile/ethanol mixture. (c) CARS signal intensity of I_{2876} and I_{3073} in the mixture (red and blue triangle) and theoretical fitting curve (red and blue solid line) as a function of benzonitrile fraction in the benzonitrile/ethanol mixture.

Raman resonance peaks exist in the HW region, the Raman resonance peaks at $2835\,\text{cm}^{-1}$ and $2945\,\text{cm}^{-1}$ represent symmetric CH_3 stretching vibration CH_3 degenerate stretching in the methanol, respectively. While two Raman resonance peaks exist in the LW spectra, the Raman resonance peaks at $2075\,\text{cm}^{-1}$ and $2255\,\text{cm}^{-1}$ represent symmetric CD_3 stretching vibration CD_3 degenerate stretching in the methanol, respectively [37]. For each CARS spectra, smoothing has been performed using the moving-average method. Overall, Fig. 8 shows that the disposable fiber probe can simultaneously detect the CARS signals of C–D bonds and C–H bonds in the samples. We can simply exchange another fiber probe for different chemical bond sensing with a suitable length to connect to the system.

Figure 9 shows the LW and HW region CARS spectra of the cyclohexane/cyclohexane-d12 mixed solutions with 2:8 (solid black line), 3:7 (solid red line), and 4:6 (solid green line) mixing ratio. We took the RMS of the first 30 data points with no signal as the noise signal. In the LW region, the signal-to-noise ratios (SNR) are 14.13 dB, 9.50 dB, and 4.3 dB, respectively; in the HW region, the SNRs are 15.08 dB, 9.24 dB, and 2.53 dB, respectively. The SNR of the CARS signal for C–H bonds in the HW region is higher than that for C–D bonds in the LW region. This is due to the fact that the susceptibility of the C–H stretch vibration is about 50% higher than that of the C–D stretch vibration [38]. CARS signal intensity correlates with the intensity of excitation light. Future work will explore non-linear optical amplification methods to amplify the power of Stokes pulses to improve detection resolution and sensitivity.
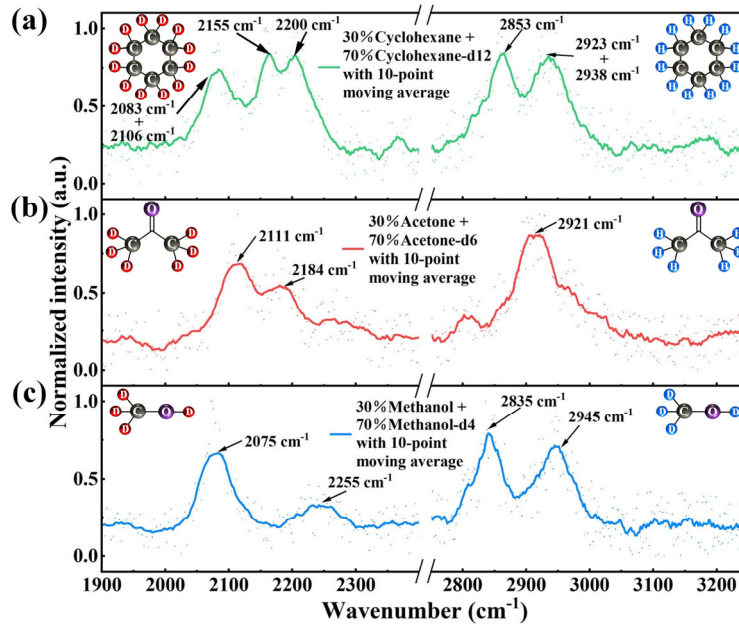
Fig. 8. CARS spectra of mixed solutions of (a) cyclohexane/cyclohexane-d12, (b) acetone/acetone-d6, and (c) methanol/methanol-d4 detected by CARS fiber probe.
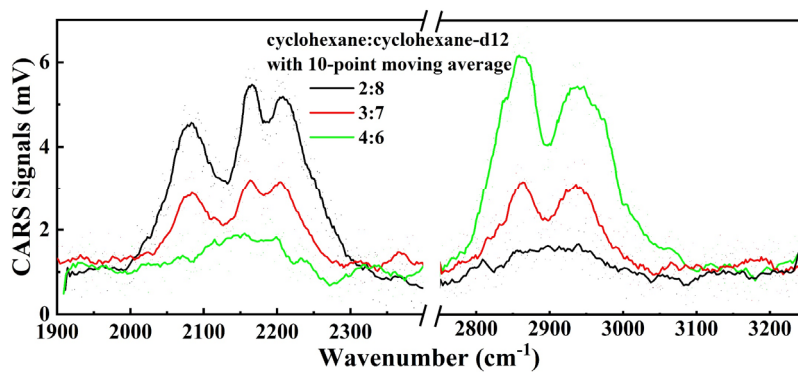

Fig. 9. CARS spectra of cyclohexane/cyclohexane-d12 mixed solutions with different mixing ratios.

4. Conclusion

In conclusion, an ultra-miniature disposable fiber probe that can simultaneously and bond-selectively detect LW and HW spectra of deuterated compounds is proposed and demonstrated. A few-mode fiber with normal dispersion is utilized and fabricated into the disposable fiber probe to deliver and align the Stokes wide-frequency-interval dual-pulse. The excitation pulses are focused by the disposable probe head, which is fabricated by the tapering process. The LW and HW region CARS signals of the samples are excited by the interaction of pump pulses with Stokes wide-frequency-interval dual-pulse. The time-domain walk-off excites between the Stokes wide-frequency-interval dual-pulse generated by the PM-PCF and is calculated and measured by characterizing standard samples. The fiber probe head with a $10.78\,\mu m$ diameter focuses the excitation pulses to the simulated cell, simultaneously detecting the Raman resonance signals of the ethanol/benzonitrile mixture in the LW region and HW region with an interval of $\sim 850\,cm^{-1}$. The measurement resolution of the Raman peaks at $2230\,cm^{-1}$, $2876\,cm^{-1}$ and $3073\,cm^{-1}$ is 0.186% (18 mM), 0.165% (28 mM), and 0.117% (11 mM). Subsequent compounds and their deuterated counterparts probe experiments demonstrate their potential for application to isotopic labeling. Subsequent detection of compounds and their deuterated counterparts demonstrated the ability of the disposable fiber probe to resolve different C–D and C–H vibrational modes and its potential for application to stable isotope labeling. Although we currently use collection fiber to collect the forward CARS signal, single-ended detection can be realized by collecting backward CARS signals and specially designed fiber. True intracellular isotope-labeled sensing can be achieved by increasing the intensity of pump light and Stokes light and thus the resolution. The simultaneous LW and HW region CARS disposable fiber probe combined with stable isotope labeling could be applied to tracking lipid metabolism in atherosclerosis plague, mapping intravascular lipid distribution, and developing drugs and monitoring treatments in the future.

Disclosures. The authors declare no conflicts of interest.

Data availability. All data needed to evaluate the conclusions are present in the paper. Additional data related to this paper may be requested from the authors.

Supplemental document. See Supplement 1 for supporting content.

References

1. B. Lorenz, C. Wichmann, S. Stockel, *et al.*, "Cultivation-Free Raman Spectroscopic Investigations of Bacteria," Trends Microbiol. **25**(5), 413–424 (2017).
2. G. R. Huys and J. Raes, "Go with the flow or solitary confinement: a look inside the single-cell toolbox for isolation of rare and uncultured microbes," Curr. Opin. Microbiol. **44**, 1–8 (2018).
3. M. Taubert, S. Stockel, P. Geesink, *et al.*, "Tracking active groundwater microbes with D(2) O labelling to understand their ecosystem function," Environ. Microbiol. **20**(1), 369–384 (2018).
4. E. J. Folco, Y. Sheikine, V. Z. Rocha, *et al.*, "Hypoxia But Not Inflammation Augments Glucose Uptake in Human Macrophages," J. Am. Coll. Cardiol. **58**(6), 603–614 (2011).
5. G. J. Koelwyn, E. M. Corr, E. Erbay, *et al.*, "Regulation of macrophage immunometabolism in atherosclerosis," Nat. Immunol. **19**(6), 526–537 (2018).
6. L. A. J. O'Neill and D. G. Hardie, "Metabolism of inflammation limited by AMPK and pseudo-starvation," Nature **493**(7432), 346–355 (2013).
7. P. Libby, J. Loscalzo, P. M. Ridker, *et al.*, "Inflammation, Immunity, and Infection in Atherothrombosis," J. Am. Coll. Cardiol. **72**(17), 2071–2081 (2018).
8. M. L. Steinhauser, A. P. Bailey, S. E. Senyo, *et al.*, "Multi-isotope imaging mass spectrometry quantifies stem cell division and metabolism," Nature **481**(7382), 516–519 (2012).
9. C. He, T. A. Weston, R. S. Jung, *et al.*, "NanoSIMS Analysis of Intravascular Lipolysis and Lipid Movement across Capillaries and into Cardiomyocytes," Cell Metab. **27**(5), 1055–1066.e3 (2018).

10. C. Guillermier, S. P. Doherty, A. G. Whitney, *et al.*, "Imaging mass spectrometry reveals heterogeneity of proliferation and metabolism in atherosclerosis," JCI Insight **4**(11), e128528 (2019).
11. F. W. McLafferty and F. Turecek, *Interpretation of mass spectra* (University science books, 1993).
12. L. Zhang, L. Shi, Y. Shen, *et al.*, "Spectral tracing of deuterium for imaging glucose metabolism," Nat. Biomed. Eng. **3**(5), 402–413 (2019).
13. R. J. A. Goodwin, "Sample preparation for mass spectrometry imaging: Small mistakes can lead to big consequences," J. Proteomics **75**(16), 4893–4911 (2012).
14. J. Nunez, R. Renslow, J. B. Cliff, *et al.*, "NanoSIMS for biological applications: Current practices and analyses," Biointerphases **13**(3), 03B301 (2018).
15. Y. F. Meng, C. H. Gao, Q. Lu, *et al.*, "Single-Cell Mass Spectrometry Imaging of Multiple Drugs and Nanomaterials at Organelle Level," Acs Nano **15**(8), 13220–13229 (2021).
16. K. Yang, H. Z. Li, X. Zhu, *et al.*, "Rapid Antibiotic Susceptibility Testing of Pathogenic Bacteria Using Heavy-Water-Labeled Single-Cell Raman Spectroscopy in Clinical Samples," Anal. Chem. **91**(9), 6296–6303 (2019).
17. L. Bu and J. E. Straub, "Vibrational frequency shifts and relaxation rates for a selected vibrational mode in cytochrome C," Biophys. J. **85**(3), 1429–1439 (2003).
18. W. Hong, C. W. Karanja, N. S. Abutaleb, *et al.*, "Antibiotic Susceptibility Determination within One Cell Cycle at Single-Bacterium Level by Stimulated Raman Metabolic Imaging," Anal. Chem. **90**(6), 3737–3743 (2018).
19. L. Guo, C. Ye, L. Cui, *et al.*, "Population and single cell metabolic activity of UV-induced VBNC bacteria determined by CTC-FCM and D(2)O-labeled Raman spectroscopy," Environ. Int. **130**, 104883 (2019).
20. C. Matthaus, C. Krafft, B. Dietzek, *et al.*, "Noninvasive imaging of intracellular lipid metabolism in macrophages by Raman microscopy in combination with stable isotopic labeling," Anal. Chem. **84**(20), 8549–8556 (2012).
21. C. Stiebing, C. Matthaus, C. Krafft, *et al.*, "Complexity of fatty acid distribution inside human macrophages on single cell level using Raman micro-spectroscopy," Anal. Bioanal. Chem. **406**(27), 7037–7046 (2014).
22. X. Yuan, Y. Song, Y. Song, *et al.*, "Effect of Laser Irradiation on Cell Function and Its Implications in Raman Spectroscopy," Appl Environ Microbiol **84**(8), e02508 (2018).
23. N. P. Ivleva, P. Kubryk, and R. Niessner, "Raman microspectroscopy, surface-enhanced Raman scattering microspectroscopy, and stable-isotope Raman microspectroscopy for biofilm characterization," Anal. Bioanal. Chem. **409**(18), 4353–4375 (2017).
24. S. You, Y. Liu, Z. Arp, *et al.*, "Intracellular imaging of docosanol in living cells by coherent anti-Stokes Raman scattering microscopy," J. Biomed. Opt **22**(7), 070502 (2017).
25. E. C. Rentchler, R. Xie, R. Hui, *et al.*, "Two-frequency CARS imaging by switching fiber laser excitation," Microsc. Res. Tech. **81**(4), 413–418 (2018).
26. I. Aporta, M. A. Quintela, and J. M. Lopez-Higuera, "Switchable Dual-Wavelength Mode-Locked Fiber Laser Source for In-PCF Parametric Frequency Conversion Applied to CARS Microscopy," J. Lightwave Technol. **37**(14), 3510–3516 (2019).
27. K. Chen, T. Wu, H. Wei, *et al.*, "Quantitative chemical imaging with background-free multiplex coherent anti-Stokes Raman scattering by dual-soliton Stokes pulses," Biomed. Opt. Express **7**(10), 3927–3939 (2016).
28. K. Chen, T. Wu, T. A. Zhou, *et al.*, "Cascaded Dual-Soliton Pulse Stokes for Broadband Coherent Anti-Stokes Raman Spectroscopy," IEEE Photonics J. **8**(6), 1–8 (2016).
29. T. Wu, K. Chen, H. Zhao, *et al.*, "Flexible dual-soliton manipulation for coherent anti-Stokes Raman scattering spectroscopy," Opt. Express **26**(17), 22001–22010 (2018).
30. Z. Wang, Y. Liu, C. Gong, *et al.*, "Liquid crystal-amplified optofluidic biosensor for ultra-highly sensitive and stable protein assay," Photonix **2**(1), 18 (2021).
31. P. Niu, J. Jiang, K. Liu, *et al.*, "High-sensitive and disposable myocardial infarction biomarker immunosensor with optofluidic microtubule lasing," Nanophotonics **11**(14), 3351–3364 (2022).
32. Y. N. Zhang, J. F. Jiang, K. Liu, *et al.*, "Dual-Frequency CARS Excitation Source With Two Independent-Tunable Stokes Wavelengths Using PM-PCF and Vector Adjustment," J. Lightwave Technol. **38**(8), 2392–2399 (2020).
33. G. P. Agrawal, *Applications of nonlinear fiber optics* (Elsevier, 2001).
34. Y. Saktioto, V. Zairmi, Veriyanti, *et al.*, "Birefringence and Polarization Mode Dispersion Phenomena of Commercial Optical Fiber in Telecommunication Networks," J. Phys.: Conf. Ser. **1655**(1), 012160 (2020).
35. T. Wang, J. F. Jiang, K. Liu, *et al.*, "Flexible minimally invasive coherent anti-Stokes Raman spectroscopy (CARS) measurement method with tapered optical fiber probe for single-cell application," Photonix **3**(1), 11 (2022).
36. Y. N. Zhang, J. F. Jiang, S. Wang, *et al.*, "Femtosecond Pulse Temporal Overlap Estimation and Adjustment in SSFS-Based CARS System," Ieee Access **7**, 131317 (2019).
37. T. Shimanouchi, *Tables of molecular vibrational frequencies* (National Bureau of Standards Washington, DC, 1972).
38. D. Boorman, I. Pope, F. Masia, *et al.*, "Quantification of the nonlinear susceptibility of the hydrogen and deuterium stretch vibration for biomolecules in coherent Raman micro-spectroscopy," J. Raman Spectrosc. **52**(9), 1540–1551 (2021).